Available online at www.sciencedirect.com
SCIENCE DIRECT
Image and Vision Computing 22 (2004) 909–918
www.elsevier.com/locate/imavis

A hand-based personal authentication using a coarse-to-fine strategy

Chin-Chuan Han*

Department of Computer Science and Information Engineering, National United University, Miaoli, Taiwan, ROC

Received 12 June 2002; received in revised form 17 May 2004; accepted 18 May 2004

Abstract

Biometrics-based verification is an effective approach to personal authentication using biological features extracted from the individual. In this paper, we propose specific verification technology by making use of hand-based features. Two hand-based features, the hand geometry and the palmprint, are simultaneously grabbed by the CCD camera-based devices. Basically, geometrical features of the hands are used to roughly verify the identity. The samples possessing the confused hand shapes should be to re-check by the palmprint features. First, the crucial points and the ROI of palmprint are determined in the preprocessing stage. The hand shape features of length 11 are computed from these detected points. Next, the multi-resolutional palmprint features are extracted from the ROI and the three middle fingers. In that way the reference vectors are obtained for computing the similarity values in various resolutions. In addition, the various verified results in multiple resolutions are integrated to achieve a better performance by using the positive Boolean function (PBF) and the bootstrapping method. Experimental results were conducted to show the effectiveness of our proposed approaches.

Keywords: Personal authentication; Hand geometry; Palmprint feature; Biometric system; Coarse to fine strategy

1. Introduction

Personal authentication (PA), using biometric features [1,2], has been attracting much attention lately. Using biological features as the personal identification number (PIN) replaces the approaches using digits. In password-based systems, people use different passwords for different systems. They usually forget the passwords or confuse them. Once people forget their passwords, they have to reset all system parameters to prevent illegal use. Biometrics provide a perfect solution to overcome these problems. They possess the identical, portable, and arduous duplicate characteristics. Many researchers [1–4] involved in this field have developed lots of effective verification algorithms and have applied these techniques to many vision-based security systems. Phillips [3] summarized the advantages and disadvantages of the biometrics features used in network-based applications. The Association for Biometrics in England [4] proposed five steps to choose the proper biometrics strategies for the security requirement of systems.

In this paper, we will focus on the hand-based features for PA. Two types of hand-based features, the geometry-based features and the palmprint features, have been successfully used in many literatures. Golfarelli et al. [2] extracted the hand shape features of length 17 to verify personal identity. They set up some latches on a plane to fix the position of hands. The images of size 640 by 512 were grabbed from a CCD camera. The backlight effect was used to acquire high contrasted images. These image can be easily segmented through a constant threshold. Besides, five features of finger length, seven features of finger width, two features of palm width, and three features of hand thickness were extracted from the thresholded images. Zunkei [5] introduced a commercial product of hand geometry-based recognition and applied it to many access control systems. Joshi et al. [6] captured an image of the middle finger by using a CCD camera to generate the wide line integrated profile (WLIP) of length 472. They also used the normalized correlation function to compute the similarity values between the input sample and the reference templates.

Zhang et al. [7–10] proposed lots of verification methods for personal identification via palmprint features. They applied the datum point invariant property and the line feature matching technique to do the verification process [7]. In Ref. [8], they proposed a texture-based feature extraction method to obtain the global attributes of a palm. A dynamic selection scheme was also designed to ensure

* Tel.: +886-3-7381824; fax: +886-3-523-2315.
E-mail address: cchan@chu.edu.tw (C.-C. Han).

0262-8856/$ - see front matter © 2004 Elsevier B.V. All rights reserved.
doi:10.1016/j.imavis.2004.05.008

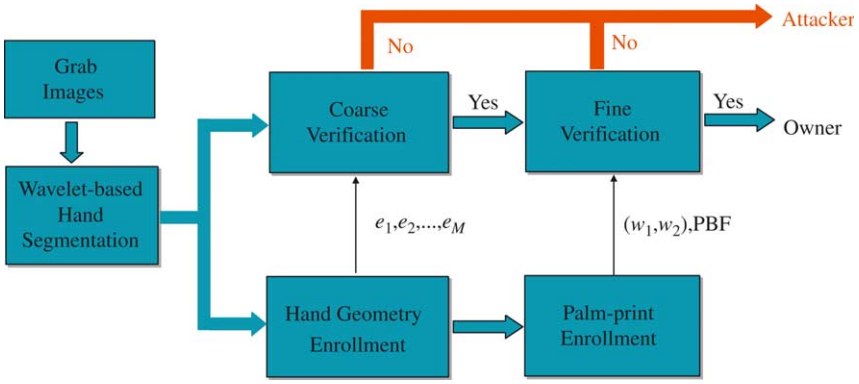

Fig. 1. The coarse-to-fine authentication system using the hand-based features.

that the palmprint samples are correctly and effectively classified in a large database [8]. Moreover, they also proposed a hierarchical palmprint coding scheme for effective and efficient palmprint verification and identification in large databases [9]. Four-level features, global geometry-based key-point distance, global texture energy, fuzzy interest line, and local directional texture energy, were defined to facilitate the coarse-to-fine matching process. Furthermore, Zhang et al. [10] designed an online palmprint identification system by using the low resolution images. Two parts, including an online palmprint acquisition device and a fast recognition algorithm, were proposed in their approach. In our previous work [11], we have proposed the scanner-based capturing environment to obtain the palmprint images.

Recently, multi-modal techniques are another approach adopted by many researchers. Multiple biometric features have been used to increase the performance of authentication systems. Chibelushi et al. [12] made a review of speech-based bimodal recognition. They combined auditory and visual modalities instead of a single modality. Sanderson and Paliwal [13] also integrated the audio and visual information in a multi-modal verification system. In addition, Chatzis et al. [14] proposed three fusion schemes to combine the still face and speech features. Prabhakar and Jain [15] proposed five kinds of multi-modal biometric systems for PA. The finger print and the face features are integrated by the *multiple sensor, multiple biometric, multiple impressions, multiple finger*, and *multiple matcher* systems. These five kinds of multi-modal biometric systems can be extended for all possible biometrics features. All of their approaches improved the performance of the system with multi-modal features.

In this paper, hand-based features are utilized for PA as shown in Fig. 1. We have designed a CCD camera-based capturing device to grab the hand images as shown in Fig. 2. This device would grab the hand shape and the palmprint features simultaneously. First of all, users are asked to put their right hand on the platform. The hand images are captured by a CCD camera in the image-grabbing module. These images are next segmented by making use of the wavelet-based segmentation method. Two stages, *enrollment* and *verification*, should be executed in authentication systems. Two kinds of hand-based features, including the hand geometry and the palmprint features, are extracted from the hand images in the enrollment stage. In the verification stage, the coarse-to-fine strategy is utilized to verify the input samples. The hand shape and the region of interest (ROI) of palmprint are automatically extracted according to the geometrical properties of the hand. For the coarse-level verification strategy, the hand-shape features of length 11 are extracted in the hand-geometry enrollment module. The palmprint features of length 500 in four scales are extracted from the ROI by using wavelet-based decomposition approaches. In the fine-level verification stage, the palmprint features of different scales are matched with the corresponding reference templates. And then these verified results are integrated to obtain the efficient performance by using an optimal PBF.

The rest of this paper is organized as follows. In Section 2, the hand images are segmented to find the locations of the fingertips and the ROI of palmprint by using the wavelet-based segmentation algorithm. The hand geometrical features of length 11 are extracted next and verified in Section 3. In Section 4, the palmprint features are obtained for the fine-level verification task by using

Fig. 2. The hand-based capturing device.

the multiple scale fusion strategy. These palmprint features represented in four scales are extracted from the three middle fingers and the ROI. The principal component analysis (PCA) and the generalized learning vector quantization (GLVQ) techniques are reviewed and utilized to generate the two-class centers in various scales. Finally, the verified results in various scales are integrated to generate the efficient verified results via the optimal PBF. Some experimental results were implemented in Section 5 to show the effectiveness of our proposed approaches. Finally, the conclusions are given in Section 6.

2. Wavelet-based hand segmentation

Image quality is the key ingredient in many pattern recognition systems. The better the image quality, the more effective the system will be. Moreover, designing the verification algorithm does not need much effort. In this paper, we designed a CCD camera-based capturing device as shown in Fig. 2. This device can simultaneously capture the hand shape and the palmprint features. We developed a wavelet-based segmentation algorithm to automatically segment the hand image and locate the fingertips and the ROI of palmprint. This algorithm finds the edge points of the hand or fingers by using the wavelet transform. As we know, the edge points locate at the zero-crossing points of the second derivation of the original signal. Wen et al. [16] utilized this technique to segment the on-line signature patterns. Based on the segmented and detected edge points, the geometrical features of hands are given in this section.

Consider the hand image as shown in Fig. 3, six sticks were previously fixed manually at $S_0, S_1, \ldots, S_5$, their corresponding coordinates being $(x_{S0}, y_{S0}), (x_{S1}, y_{S1}), \ldots, (x_{S5}, y_{S5})$. Next, the edge points of the three middle fingers (e.g. the index finger, the middle finger, and the ring finger) were found for the segmentation of the hand images. In our experiments, the profile of an arbitrary horizontal line $\overline{S_M S_N}$ (Fig. 3) is set with the equation $y = y_{S0} + 70$. The signals of this profile are transformed by the wavelet transform. Several low-frequency and high-frequency sub-band signals in various scales are generated as depicted in Fig. 4. In Wen's approaches [16], the signature patterns were segmented from the high-frequency sub-band signals at scale 4. The edge points of the fingers at line $\overline{S_M S_N}$ in Fig. 3 are found by the similar manner in the followings. Since the capturing environment is well designed and controlled, three fingers are located within the searching range [1/8,7/8] of the image width. In Fig. 4d, the zero-crossing points beyond the searching range are first eliminated. The search range is next separated into three parts based on sticks S_4 and S_5. The positions with local maximal magnitude in each part are marked. Two edge points are found at the zero-crossing points nearing to the marked position in each part. Thus, points $S_A, S_B, S_C, S_D, S_E, S_F$ in Fig. 3 are

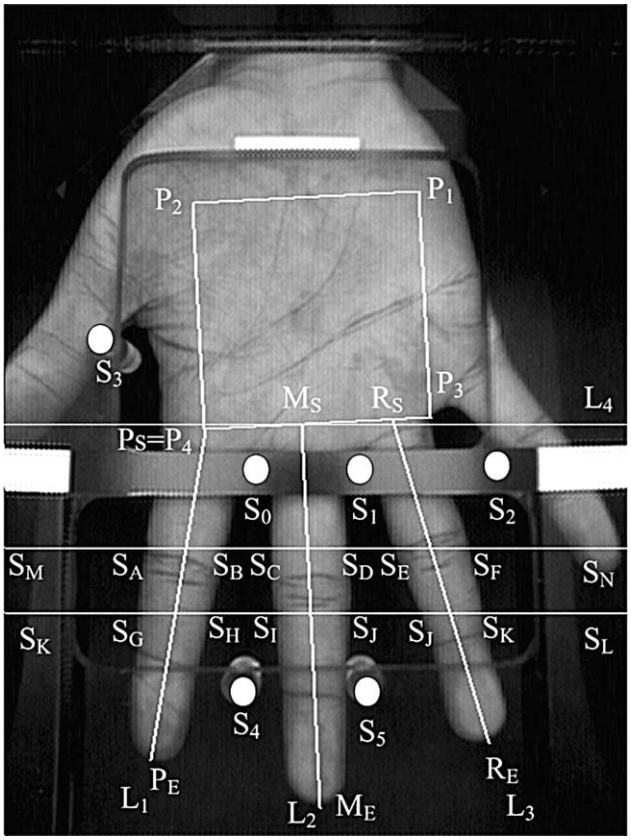

Fig. 3. The hand segmentation process.

obtained from the high-frequency sub-band signals at scale 4 in Fig. 4d. Similarly, the edge points of fingers $S_G, S_H, S_I, S_J, S_K, S_L$ in Fig. 3 can also be obtained by the above wavelet-based segmentation algorithm.

Next, the ROI $P_1P_2P_4P_3$ in Fig. 3 is automatically located according to the geometrical properties of the hand. The three central lines of fingers L_1, L_2, and L_3 are first calculated from those six segments $\overline{S_A S_B}$, $\overline{S_C S_D}$, $\overline{S_E S_F}$, $\overline{S_G S_H}$, $\overline{S_I S_J}$, and $\overline{S_K S_L}$. Secondly, the intersected point M_S is computed from lines L_2 and L_4, where L_4 is a horizontal line of $y = (y_{S3} + 2y_{S0})/3$. This is the starting point for determining the ROI of palmprint. According to our experience and careful observation, two lines $\overline{P_1P_3}$ and $\overline{P_2P_4}$ in ROI are parallel to line L_2. Line $\overline{P_3P_4}$ is also perpendicular to line L_2. Therefore, the corner point P_4 of the palm table is obtained from the intersection points of lines $\overline{P_3P_4}$ and L_1, and $P_4 = P_S$. Another intersection point of lines L_3 and $\overline{P_3P_4}$ is R_S. Thus, the palm table is defined to be a rectangular area $P_1P_2P_4P_3$, where $|\overline{P_3P_4}| = 1.2|\overline{R_SP_S}|$. In addition, the three fingertips P_E, M_E, R_E are found from the zero-crossing points of the transformed signals of lines L_1, L_2, and L_3 at scale 4, respectively. The wavelet-based segmentation algorithm is described in the followings.

Step 1: Input the coordinates of peg $S0$, i.e. (x_{S0}, y_{S0}).

Step 2: Find the edge points $S_A, S_B, S_C, S_D, S_E, S_F$ in line $\overline{S_M S_N}$.

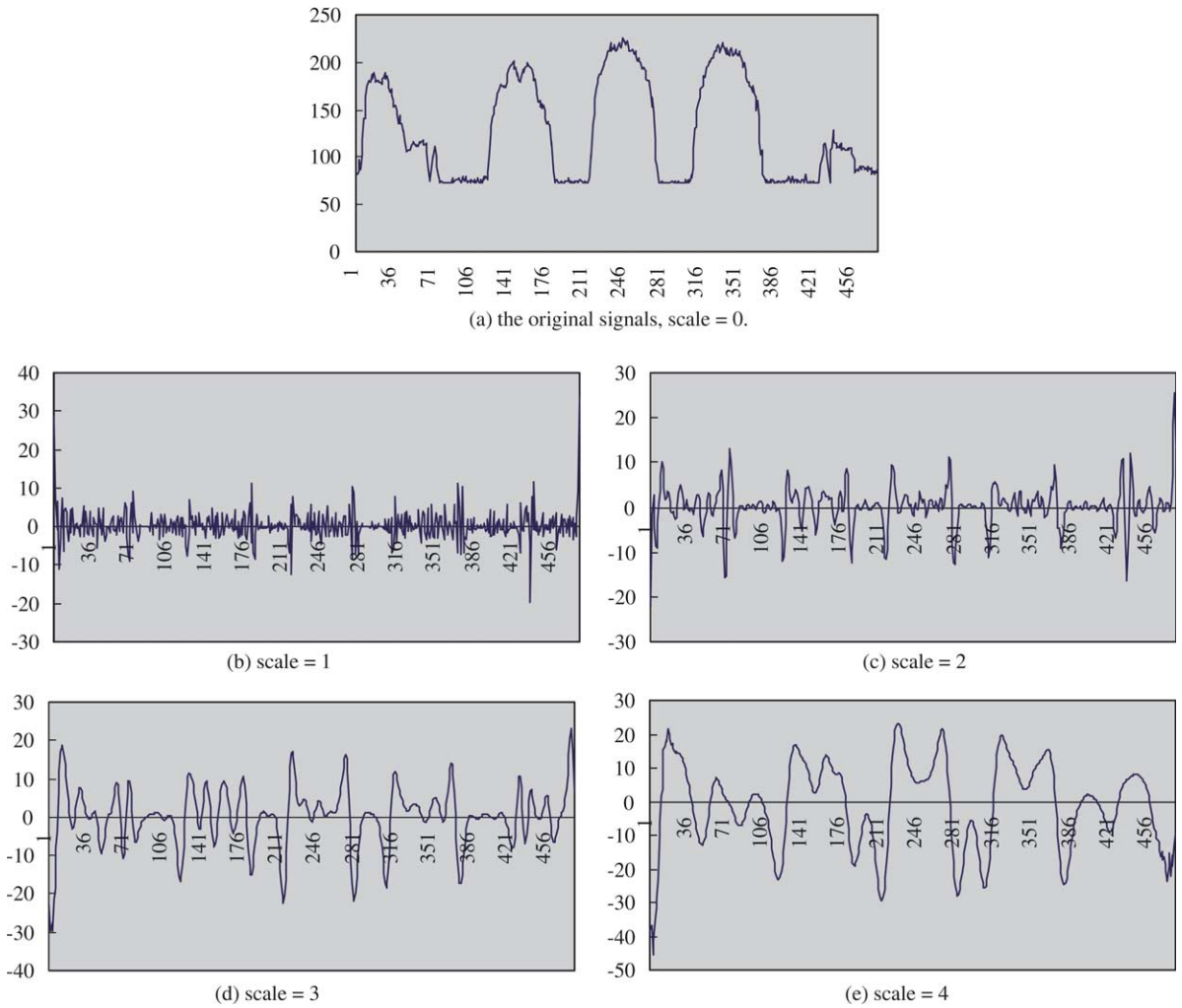

Fig. 4. (a) The original signals, scale = 0. (b)–(e) The high-frequency sub-bands of the wavelet transformed signals from scales 1 to 4.

1. Extract the profile of line $\overline{S_M S_N}$, where $\overline{S_M S_N}$: $y = y_{S0} + 70$.
2. Decompose the profile of line $\overline{S_M S_N}$ into several signals of the low-frequency sub-band Sf_i and the high-frequency sub-band Wf_i, where $i = 1, 2, 3, 4$ in this paper.
3. Find the edge points $S_A, S_B, S_C, S_D, S_E, S_F$ from the transformed signal Wf_4 at scale 4.

Step 3: Find the edge points $S_G, S_H, S_I, S_J, S_K, S_L$ from line L_4 by repeating the segmentation process in Step 2.

1. Generate the profile of the horizontal line L_5, where L_5 : $y = y_{S_0} + 130$.
2. Decompose the profile of line L_5 into several signals of the low-frequency sub-band Sf_i and the high-frequency sub-band Wf_i, where $i = 1, 2, 3, 4$.
3. Find the edge points $S_G, S_H, S_I, S_J, S_K, S_L$ from the transformed signal Wf_4 at scale 4.

Step 4: Compute three equations of the lines L_1, L_2, and L_3 from these 12 points $S_A, S_B, \ldots, S_L$.

Step 5: Compute the intersection points P_S, M_S, and R_S from lines L_1, L_2, L_3 and L_4, respectively, where $L_4 : y = (2y_{S0} + y_{S3})/3$.

1. Determine the location of the point M_S which is intersected by lines L_2 and L_4.
2. Compute the equation of line $\overline{P_3P_4}$ from point M_s and line L_2, where $L_2 \perp \overline{P_3P_4}$.
3. Find the intersection points P_S and R_S from lines $\overline{P_3P_4}$ and L_1, $\overline{P_3P_4}$ and L_3, respectively.

Step 6: Determine the four coordinates of ROI $P_1P_2P_3P_4$ from two points P_S and R_S, where $|P_3P_4| = 1.2|R_sP_s|$.

3. Coarse-level verification using hand geometrical features

PA using hand geometrical features provides an effective performance in biometrics-based security systems.

However, the geometrical shapes of hands will vary significantly over time due to the wearing of rings, the finger mails, or the pregnancy of women. Moreover, similar and confused hand shapes of different individuals are other factors making the hand geometry-based authentication systems be used in a small database.

In this section, we reduce the false rejection rate (FRR) to increase the tolerance of the change of hand shape by checking the input samples in the looser criteria. Then, the palmprint features as stated in Section 4, are adopted to do the stricter verification task. This will reduce the mis-verification error caused by the time factor.

Fig. 5 shows a hand image in which eleven geometrical features are obtained from the wavelet-based segmentation and the geometrical formulas. In these features, lines $\overline{P_AP_B}$ and $\overline{P_CP_D}$ are perpendicular to line $\overline{P_EP_F}$. Besides, lines $\overline{P_AP_B}$ and $\overline{P_CP_D}$ are located at 1/3 and 2/3 places of line $\overline{P_EP_F}$, respectively. The lengths of lines $\overline{P_AP_B}$, $\overline{P_CP_D}$, and $\overline{P_EP_F}$ are set to be the features 1, 2, and 3. Similarly, features 4, 5,…,9 can be generated from the above procedure. In addition, the lengths of lines $\overline{P_GP_H}$ and $\overline{P_IP_J}$ represent the 10th and 11th features, respectively. Here, $|\overline{P_2P_I}| = 0.25|\overline{P_2P_4}|$, $\overline{P_IP_J} \perp \overline{P_3P_4}$, and $|\overline{P_3P_4}|$ is the ROI width of palmprint. The value 0.25 is an arbitrary value smaller than 0.5 to find the edge point P_J of the first finger. Based on points P_I and P_J, the 11th is thus obtained. Of these features, the first nine denote the finger shape and the last two denote the size of the palm table.

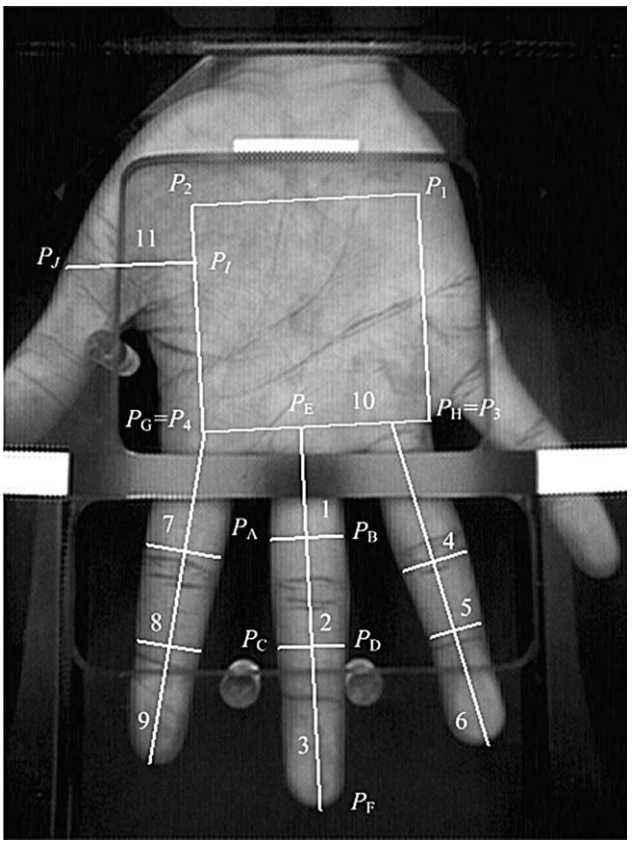

Fig. 5. Eleven hand geometrical features.

Suppose that M training samples of an individual X are collected in the enrollment stage then, from the preceding process, M vectors of length 11, denoted as $f_i = (f_{i1}, f_{i2}, \ldots, f_{i11})$, are generated, $i = 1, 2, \ldots M$. The sample mean $\mu = (\mu_1, \ldots, \mu_{11})$ and the covariance matrix $\Sigma = \mathrm{diag}(\sigma_1^2, \sigma_2^2, \ldots, \sigma_{11}^2)$ are computed from these M vectors, respectively. In the coarse-level verification module, the Mahalanobis distance defined in Eq. (1) is used to evaluate the similarity between the input sample and the mean of templates.

$$d^2 = (\mathbf{x} - \mu)^t \Sigma^{-1} (\mathbf{x} - \mu) = \sum_{i=1}^{11} \left(\frac{x_i - \mu_i}{\sigma_i} \right)^2. \quad (1)$$

Here, $\mathbf{x}$ is the feature vector of an input realization. This sample is verified to determine whether it belongs to X or not.

If the distance is larger than a looser and pre-defined threshold, the input sample is classified as being an attacker. Otherwise, this sample would be re-checked in the palmprint-based verification.

Since the capturing environment is well controlled, the detection of edge points of fingers is very effective in the previous section. The features of fingers are sometimes varied due to the long finger mails. To solve this problem, the coarse-to-fine scheme is proposed in this paper. In the coarse-level verification phase, the tolerance is considered by a looser threshold. If the testing sample passes the above looser criterion, it should be rechecked by the palmprint feature in the fine-level verification phase.

4. Fine-level verification using the palm-print features

When the input sample x satisfies the threshold value by using the hand geometrical features in the coarse-level verification module, it should be re-checked via the palmprint features in the fine-level verification module. In this section, we will extract the multi-resolutional palmprint features from the three middle fingers and the ROI. The dimensionality of these features should be reduced for the simplification of the classifier design by the PCA approach. Next, the GLVQ technique is applied to re-check the input sample. Finally, an optimal positive Boolean function (PBF) will be found to combine the verified results in various scales.

4.1. Feature extraction in multiple scales

Before stating the extraction process of the palmprint features, let us summarize the PCA technique. Suppose there are M training samples possessing the feature vectors of length L then, the covariance matrix M_c is defined as

$$M_c = \sum_{i=1}^{M} (x - \mu)(x - \mu)', \quad (2)$$

where μ denotes the sample mean. The major K eigenvectors e_i corresponding with the largest K eigenvalues λ_i comprise a K-dimensional sub-space called

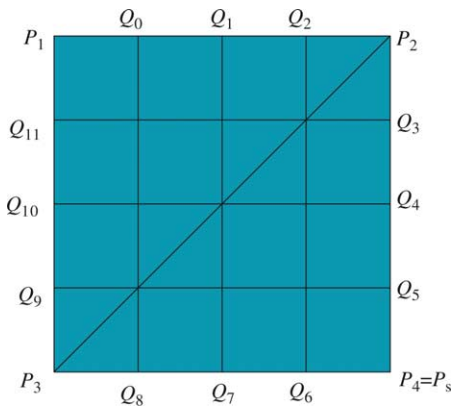

Fig. 6. Seven palm-print features.

eigenspace, where $K \ll L$. And, the rest of the eigenvectors organize the residual subspace. Thus, the original space is decomposed into two subspaces. A realization x of length L can be projected into the eigenspace to obtain a new vector $V = [e_1, e_2, \ldots, e_K]^T(x - \mu)$. The original vector of length L is represented by a new vector of length K, called distance in feature space (DIFS). Turk and Pentland [17] applied this approach to reduce the dimensionality of feature vectors for face recognition. Hong and Jain [1] used the residual error (DFFS) function to solve the face verification problem.

As described in the preceding sections, the ROI of palmprint is automatically located in the hand segmentation procedure. The palmprint features of multiple resolutions are subsequently extracted from the ROI. In pattern recognition, images are usually concatenated row by row to obtain

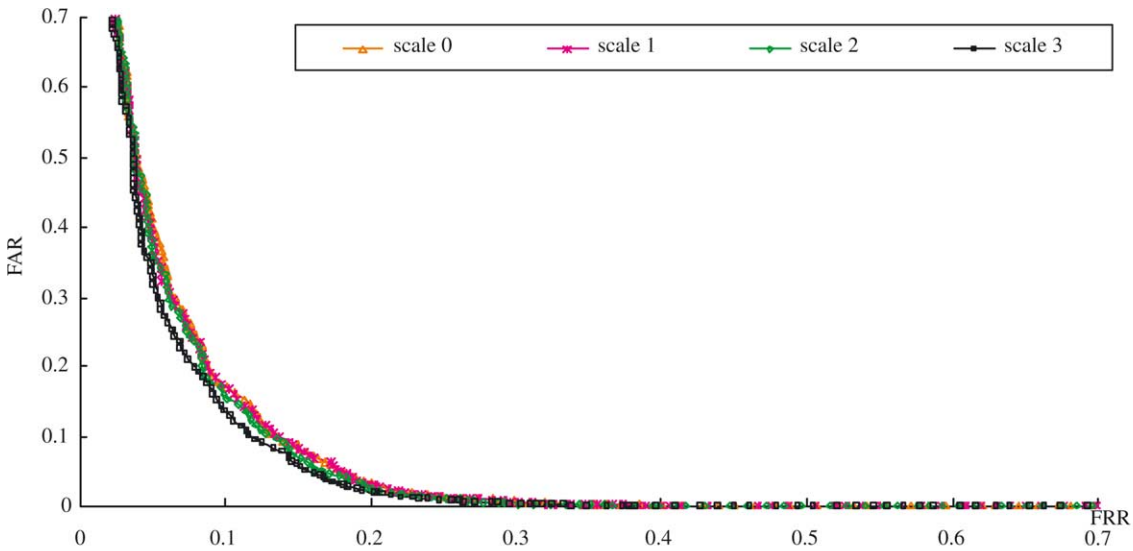

(a) 4 low-frequency sub-bands

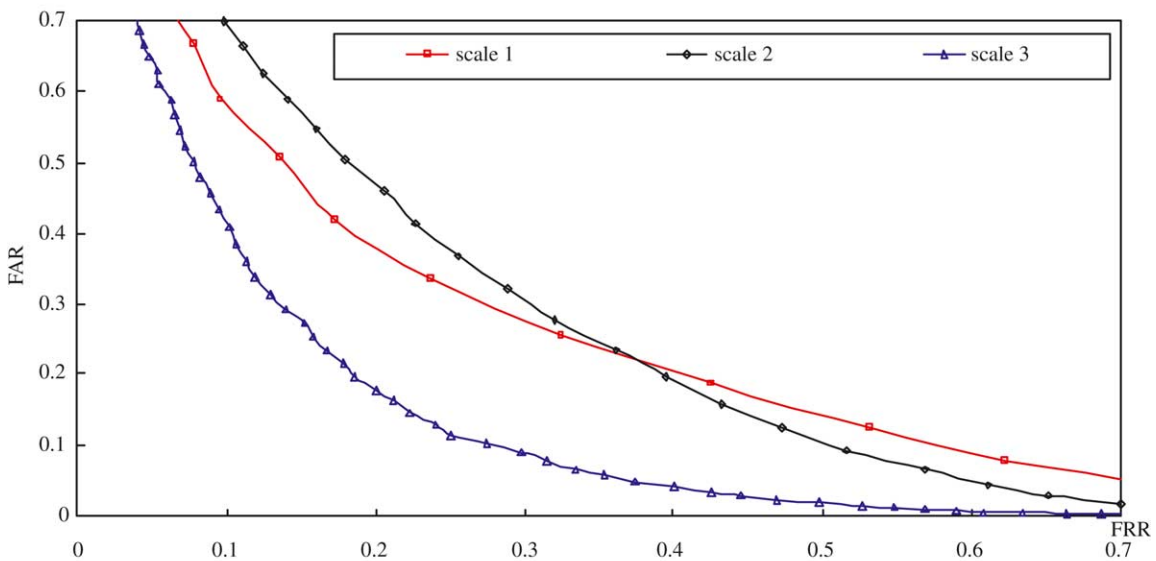

(b) 3 high-frequency sub-bands

Fig. 7. The ROC of the verification results using palmprint features in various low-frequency and high frequency sub-bands.

the feature vectors. However, the dimensionality of feature vectors of the whole image is too high to decrease the complexity of classifier design. In this study, the palmprint images are sub-sampled to obtain the profile of scanning line for the dimensionality reduction. The profiles of seven specified lines in ROI, as shown in Fig. 6, are extracted. Since there are lots of redundant data in this area, seven lines $\overline{Q_0Q_8}$, $\overline{Q_1Q_7}$...$\overline{Q_5Q_9}$, and $\overline{P_2P_3}$ are specified to extract the feature vectors and used to represent the palmprint. It is worth noting that line $\overline{P_1P_4}$ is not taken into consideration because point P_1 is frequently located in the background. The background pixels will be embedded in the profile of line $\overline{P_1P_4}$. In the profile of line $\overline{P_2P_3}$, for example, the signals in the multi-scales (Fig. 8) were generated by using the wavelet transforms. Etemad and Chellappa [18] analyzed the transformed signals of the face to compute the discriminant power. In order to evaluate the discriminant power of palmprint features in various sub-bands, an experiment was performed. In this experiment, original signals were decomposed into four low-frequency sub-bands and three high-frequency sub-bands. The template matching strategy was adopted to calculate the distances between querying samples and templates in verification process. The receiver operating characteristics (ROC) curves are shown in Fig. 7. From this figure, the discriminant power of the high-frequency sub-band Wf_i is less than that of the low-frequency sub-band Sf_i. Therefore, the signals of the high-frequency sub-band Wf_i are ignored in this paper. The low-frequency sub-band signals Sf_i of line $\overline{P_2P_3}$ at scale i are normalized and defined to be the feature vectors of the palmprint of length L. Furthermore, seven feature vectors of length L are catenated to denote the palmprint features of a specified individual at scale i (Fig. 8).

In addition, the three middle fingers also include the discriminant power. The profiles of these three fingers are transformed and normalized to be three feature vectors of length L. These 10 vectors are catenated to form a new feature vector of length $10L$ at scale i to denote the palmprint feature of an individual. Next, dimensionality reduction is needed to reduce the complexity of the verification algorithm by using the PCA methods. The reduced feature vectors can be transmitted very fast in network-based biometric verification applications. The original feature vectors of length $10L$ can be projected to obtain a vector of length K at a specified scale i. R feature vectors Rf_i of length K can be obtained with $i = 1, 2, \ldots R$. Here, value K is set to 50 in this study since the first 50 components would contain more than 95% information of the original data.

4.2. Generalized learning vector quantization

The main work in PA is to verify whether the input sample belongs to an individual X or not. This is a two-category classification problem. In this subsection, two category centers, called centers 'YES' (ω_1) and 'NO' (ω_2), are determined by using the GLVQ method.

Assume that M training samples of an individual X are collected and denoted as the data set $\mathscr{D}_X$. MN samples which are randomly selected from another N persons are collected

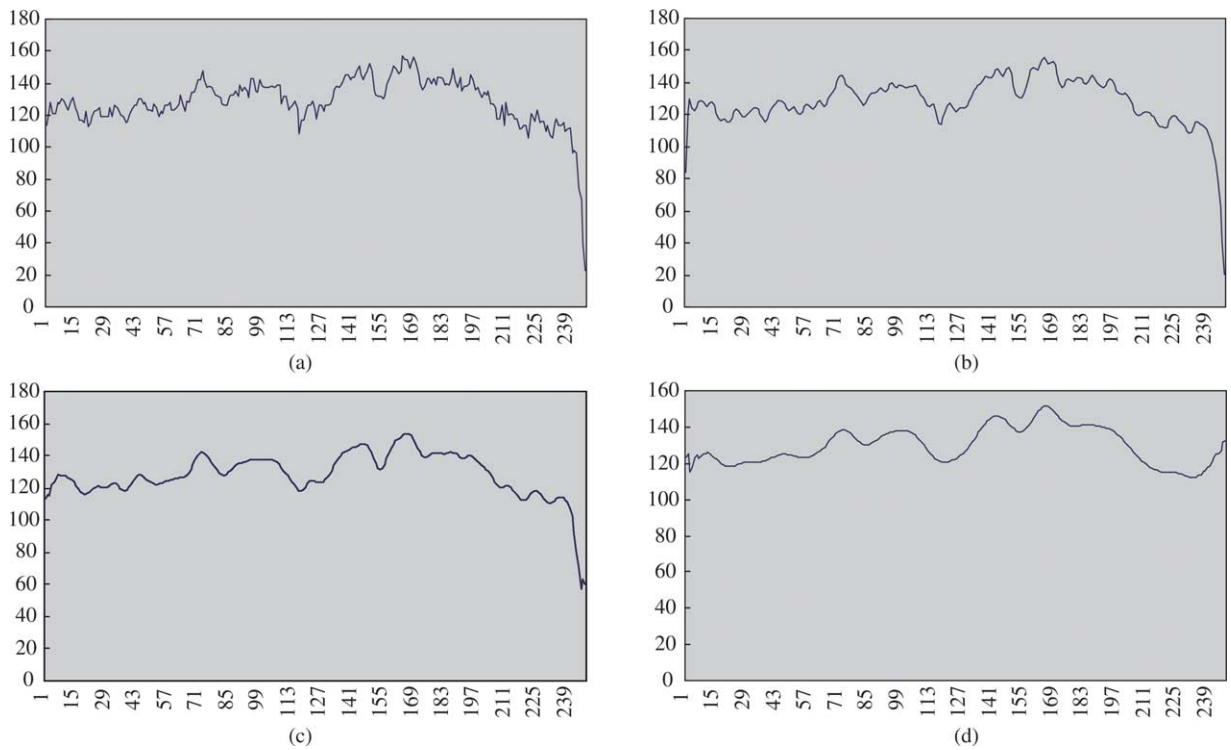

Fig. 8. The low-frequency sub-band signals of line $\overline{P_2P_3}$ from scales 0 to 3.

to form the non-X data set $\mathscr{D}_{\bar{X}}$. In the GLVQ training process, since the training samples in the data set $\mathscr{D}_X$ are relatively few as opposed to those in non-X data set $\mathscr{D}_{\bar{X}}$, M samples of the individual X should be duplicated N times to generate MN instances for the simplification of implementation. Plus the MN instances from another N persons, $2MN$ instances are interlacedly inputted into the GLVQ process to generate two category centers ω_1 and ω_2. The GLVQ algorithm is the general case of learning vector quantization (LVQ) method which was proposed by Kohonen [19]. Many versions of GLVQ have been proposed from different viewpoints [20–22]. In this paper, we adopted Sato's approach [20] to generate the two best category centers. The updating rules for Sato's method is briefly described below.

Consider a training sample x and two category centers ω_1 and ω_2. The relative distance function $\mu(x)$ is defined as

$$\mu(x) = \frac{d_1 - d_2}{d_1 + d_2}, \tag{3}$$

where $d_1 = |x - \omega_1|^2$ and $d_2 = |x - \omega_2|^2$ are the squared Euclidean distances for the sample x to centers ω_1 and ω_2, respectively.

Suppose that center ω_1 is the nearer center for the sample x and they belong to the same class, i.e. $\mathbf{class}(x) = \mathbf{class}(\omega_1)$. The updating rule for center ω_1 is designed as

$$\omega_1(t+1) = \omega_1(t) + \alpha \frac{\partial f}{\partial \mu} \frac{d_2}{(d_1 + d_2)^2}(x - \omega_1(t)). \tag{4}$$

On the other hand, if center ω_2 is the nearer center for the sample x but they do not belong to the same class, i.e. $\mathbf{class}(x) \neq \mathbf{class}(\omega_2)$, then the learning rule for center ω_2 is designed in the following formulation.

$$\omega_2(t+1) = \omega_2(t) - \alpha \frac{\partial f}{\partial \mu} \frac{d_1}{(d_1 + d_2)^2}(x - \omega_2(t)). \tag{5}$$

Here, $\partial f/\partial \mu = f(\mu, t)(1 - f(\mu, t))$ in the above two equations are defined to be a gain fact. $f(\mu, t) = 1/(1 + e^{-\mu t})$ is a sigmoid function and value α is set to be 0.001 in this paper. The readers can refer more details in Ref. [20].

In principle, if an input sample x is nearer to the class center ω_1, i.e. $\mu(x) < 0$, it can be considered as the hand image of person X. Otherwise, this input sample x should be classified as an attacker's hand image. In the enrollment stage, all $2MN$ training samples are processed by the hand segmentation, the feature extraction, and the GLVQ modules to obtain R two-category centers $(\omega_1, \omega_2)_1, (\omega_1, \omega_2)_2, \ldots$, and $(\omega_1, \omega_2)_R$ in R scales. The input sample x possessing R palmprint feature vectors $Rf_1, Rf_2, \ldots Rf_R$ will match with R two-category centers to obtain the R distance values $\mu(x)_1, \mu(x)_2, \ldots, \mu(x)_R$. These R distance values are used to determine the verified results by the above principle. The verification results for ten persons at four scales are shown in Table 1. In this table, the values represent the false rejection rate (FRR) and the false acceptance rate (FAR) in each cell, respectively. The experiment will be stated in more detail in Section 5. Consider the verified results for two individuals X and Y as shown in Table 1, the verified results of identity X at scale 0 or scale 3 are better than those at the other scales. The results of Y at scale 2 are the best verified results in all scales. In the next subsection, an optimal PBF for a specified individual X will be found to integrate the various verified results and increase the verification performance.

4.3. Integration via positive boolean function(PBF)

PFB has been successfully applied on the design of stack filters. The main function for stack filters is to remove the noises, detect the edges, etc. They are only used in image processing or signal processing fields. In this section, we will use the PBF to integrate the verified results in various scales. We briefly review the operation of PBF below.

Wendt et al. [23] have shown that a stack filter can be represented by a corresponding PBF. The PBF is exactly one sum-of-product form without any negative components. For instance, the PBF of $f(x_1, x_2, x_3) = x_1x_2 + x_2x_3 + x_3x_1$ is a median function of an observation window of three variables. Let X_n of length n be the signal processed using a stack filter $S_f(\cdot)$. The signal X_n can be decomposed into $L - 1$ binary signals $X_n^l = (x_1^l, x_2^l, \ldots x_n^l) \in \{0, 1\}^n$ by using

Table 1
The verification results at various scales

ID	Scale 0	Scale 1	Scale 2	Scale 3
Y, 0	(20.00%,0.00%)	(13.33%,0.00%)	(6.67%,0.74%)	(6.67%,1.48%)
1	(0.00%,0.00%)	(0.00%,0.00%)	(0.00%,0.00%)	(6.67%,0.00%)
2	(0.00%,0.00%)	(6.67%,0.00%)	(6.67%,0.74%)	(6.67%,4.44%)
3	(86.67%,0.00%)	(73.33%,0.00%)	(73.33%,0.00%)	(73.33%,0.00%)
X, 4	(6.67%,0.74%)	(6.67%,2.96%)	(6.67%,3.70%)	(6.67%,0.74%)
5	(0.00%,0.74%)	(0.00%,0.74%)	(0.00%,0.74%)	(20.00%,0.00%)
6	(13.33%,0.00%)	(33.33%,0.00%)	(33.33%,0.00%)	(20.00%,0.00%)
7	(53.33%,0.00%)	(33.33%,1.48%)	(26.67%,5.19%)	(20.00%,5.19%)
8	(0.00%,0.00%)	(0.00%,0.00%)	(0.00%,0.00%)	(6.67%,0.00%)
9	(26.67%,0.00%)	(26.67%,0.00%)	(26.67%,0.00%)	(26.67%,0.74%)

the threshold function as follows.

$$x_i^l = T_l(x_i) = \begin{cases} 1 & \text{if } x_i \geq l, \\ 0 & \text{else} \end{cases}. \tag{6}$$

Based on the threshold decomposition property, the output value of the stack filter $S_f(X)$ can be obtained from the summation of the binary values generated from the PBF $f(\cdot)$ in the following formula:

$$S_f(X_n) = S_f\left(\sum_{l=1}^{L-1} X_n^l\right) = \sum_{l=1}^{L-1} f(X_n^l). \tag{7}$$

Wendt et al. [23] have shown that the necessary and sufficient condition for a Boolean function to possess stacking property is that it must have a PBF. An n-input Boolean function $f(\cdot)$ is said to possess *stacking property* if

$$f(x_1^l, x_2^l, \ldots, x_n^l) \geq f(y_1^l, y_2^l, \ldots y_n^l) \tag{8}$$

when $x_i^l \geq y_i^l$ for all i, and $l = 1, \ldots, L-1$.

The mean absolute error (MAE) value $C(S_f)$ which is the measurement between the outputs of the stack filter $S_f(W(\cdot))$ and the desired signal $S(\cdot)$, can be defined as

$$C(S_f) = E[|S(\cdot) - S_f(W(\cdot))|], \tag{9}$$

where $W(\cdot)$ is the input signal. According to the stacking and the threshold decomposition properties [24], the multi-level MAE is decomposed into the sum of the absolute errors incurred on each of the levels and defined as follows.

$$\begin{aligned} C(S_f) &= E\left[\left|\sum_{i=1}^{L-1} s_i(t) - f(w_i(t))\right|\right] \text{(by threshold decomposition)} \\ &= E\left[\sum_{i=1}^{L-1} |s_i(t) - f(w_i(t))|\right] \text{(by stacking property)} \\ &= \sum_{i=1}^{L-1} E[|s_i(t) - f(w_i(t))|], \end{aligned} \tag{10}$$

in which, value $L = 256$ is the quantized number in a gray image, and f is a PBF. The binary values $s_i(t)$ and $w_i(t)$ are the output values of a threshold function at position t in a gray image. The optimal stack filter is defined as a PBF which can minimize the MAE between the desired and the output signals.

The problem of integrating the verification results is reduced to the problem of finding an optimal PBF. The verified results at a specified scale can be considered as a binary random variable. The distance vector of a sample is considered as a realization x and quantized into L levels ($L = 1000$). This distance vector can be converted to binary vectors by the thresholding function. In the supervised training stage, the training samples were used whose identities were known and predefined. If sample x belongs to an individual X, the desired value is set to be zero. Otherwise, if sample x belongs to class non-X, $\mathscr{D}_{\bar{X}}$, the desired value of sample x is one. The integration function is defined to be a PBF. The classification errors as defined in Eq. (10) will occur at (1) the samples not belonging to class $\mathscr{D}_X$ being classified as the elements of class $\mathscr{D}_X$, i.e. $s(\cdot) = 1$, $f(\cdot) = 0$; or (2) the samples belonging to class $\mathscr{D}_X$ not being the elements of class $\mathscr{D}_X$, i.e. $s(\cdot) = 0$, $f(\cdot) = 1$. The best classifier can be generated from the optimal PBF with the minimal classification errors incurred at all levels. In finding the optimal PBF, both training samples in classes $\mathscr{D}_X$ and $\mathscr{D}_{\bar{X}}$ were equally created for the simplification of implementation. Since the samples in class $\mathscr{D}_X$ are relatively few as opposed to those in class $\mathscr{D}_{\bar{X}}$, some extra samples for class $\mathscr{D}_X$ were generated by the bootstrap methodology for the accuracy of PBF. MN artificial generating samples were created by duplicating M samples N times for individual X. Another MN samples were also randomly selected from N another persons to generate the same sample size of classes $\mathscr{D}_X$ and $\mathscr{D}_{\bar{X}}$. These $2MN$ samples were inputted in the search of optimal PBF. Here, values M and N are, respectively, set to be 10 and 20 in this study. In the duplication process, the ROI $P_1P_2P_4P_3$ is randomly rotated by -5 to 5°, resized by 97–103%, and shifted in x or y axis by -2 to 2 pixels. The palmprint features in multiple resolutions are obtained from the process as stated in the preceding contexts. R distances in R scales are inputted to the optimal PBF. The output of the optimal PBF will be the integration results of the distances in various scales.

However, finding the optimal PBF needs lots of computational time because that a large number of PBFs have to be checked. A fast method was proposed in our previous work for finding the optimal stack filter (i.e. an optimal PBF). More details can be referred in reference [25].

5. Experimental results

In this section, some experimental results were implemented to show the effectiveness of our proposed methods. A database was constructed by collecting 1500 hand images from 50 persons. This database was constructed over one year. In average, the images per person were grabbed during two months. These images were all grabbed from the students or teachers in university by CCD camera-based devices. Most of them are male in the constructed database. In the experiments, 10 images of a person were randomly selected and used to train the model in the enrollment stage, and the other 20 images were used to test the performance of our approaches. Each image was processed by the hand segmentation, the ROI locating of palmprint, and the feature extraction of hand geometry, to obtain the feature vectors of length 11. The similarity values between the input samples and the reference templates were calculated next. In the verification process, 20 test images of a specified person X were tested to calculate the FRR value, and the images of other persons (980 images of 49 persons) were used to calculate the FAR value. The threshold value for the coarse-level (hand geometry) verification module

was set to be 4. The performance for these 50 persons is FRR = 1.6% and FAR = 36.3%. In the fine-level verification stage, four feature vectors of length 500 from scales 0 to 3 were reduced to the vectors of length 50 by using the PCA method. The image samples of a considered individual X (positive samples) plus those samples of another 20 persons (negative samples) were collected to obtain the reference vectors in four scales by making use of the GLVQ approach. The verified results for the specified individual in four scales were integrated to obtain a final verification result via an optimal PBF. The FRR and FAR values for 50 persons using the palmprint features are 4.0 and 9.1%, respectively. Finally, the coarse-level (hand geometry) and the fine-level (palmprint) verification modules were sequentially combined to obtain the results of FFR = 5.3% and FAR = 3.7%.

6. Conclusion

In this paper, two hand-based features have been adopted for PA. The statistical features of palmprint are extracted and matched with a coarse-to-fine verification scheme. The experimental results have been demonstrated to show the effectiveness of our proposed approach. In the future, the restriction of capturing devices, i.e. sticks, will be removed for more users such as the children. Without this restriction, the effective algorithms for locating the ROI of palmprint are needed. The palmprint images will be segmented to obtain the lines and verified by the effective matching algorithms.

Acknowledgements

The database used in this paper is supported by Chunghwa Telecommunication Laboratories under grant no. TL-89-5013. The author would also like to thank Dr P.C. Chang and Mr C.C. Hsu for their constructive comments.

References

[1] L. Hong, A.K. Jain, Integration faces and fingerprints for personal identification, IEEE Transactions on Pattern Analysis and Machine Intelligence 20 (12) (1998) 1295–1307.
[2] M. Golfarelli, D. Miao, D. Maltoni, On the error-reject trade-off in biometric verification systems, IEEE Transactions on Pattern Analysis and Machine Intelligence 19 (7) (1997) 786–796.
[3] K. Phillips, Biometric identification looms on landscape of network log-ins: high-end technology is becoming more affordable, PC Week (1997).
[4] AFB, A five step guide to selecting a biometric system, Association for Biometrics, 1999, biometric.
[5] R.L. Zunkei, Hand geometry based verification, in: A.K. Jain, R. Bolle, S. Pankanti (Eds.), Biometrics: Personal Identification in Networks Society, Kluwer Academic Publishers, Dordrecht, 1999, pp. 87–101, chapter 4.
[6] D.G. Joshi, Y.V. Rao, S. Kar, V. Kumar, R. Kumar, Computer-vision-based approach to personal identification using finger crease pattern, Pattern Recognition 31 (1) (1998) 15–22.
[7] D. Zhang, W. Shu, Two novel characteristics in palm-print verification: Datum point invariance and line feature matching, Pattern Recognition 32 (1999) 691–702.
[8] J. You, W. Li, D. Zhang, Hierarchical palmprint identification via multiple feature extraction, Pattern Recognition 35 (2002) 847–859.
[9] J. You, W.K. Kong, D. Zhang, K.H. Cheung, On hierarchical palmprint coding with multiple features for personal identification in large database, IEEE Transactions on Circuits and Systems for Video Technology 14 (2004) 234–242.
[10] D. Zhang, W.K. Kong, J. You, M. Wong, Online palmprint identification, IEEE Transactions on Pattern Analysis and Machine Intelligence 25 (2003) 1041–1049.
[11] C.C. Han, H.L. Cheng, C.L. Lin, K.C. Fan, C.-L. Lin, Personal authentication using palmprint features, Pattern Recognition 36 (2003) 371–382.
[12] C.C. Chibelushi, F. Deravi, J.S.D. Mason, A review of speech-based bimodal recognition, IEEE Transactions on Multimedia 4 (2002) 23–37.
[13] C. Sanderson, K.K. Paliwal, Noise compensation in a person verification system using face and multiple speech features, Pattern Recognition 36 (2003) 293–302.
[14] V. Chatzis, A.G. Borş, I. Pitas, Multimodal decision-level fusion for person authentication, IEEE Transactions on System, Man, and Cybernetics—Part A: Systems and Humans 29 (1999) 674–680.
[15] S. Prabhakar, A.K. Jain, Decision-level fusion in fingerprint verification, Pattern Recognition 35 (2002) 861–874.
[16] C.J. Wen, H.F. Yau, B.S. Jeng, Optimal segmentation of handwritten Chinese signatures using wavelet transforms, Optical Engineering 35 (9) (1996) 2721–2729.
[17] M. Turk, A. Pentland, Eigenfaces for recognition, Journal of Cognitive Neuroscience 3 (1) (1991) 71–86.
[18] K. Etemad, R. Chellappa, Discriminant analysis for recognition of human face recognition, Journal of Optical Society America 14 (8) (1997) 1724–1733.
[19] T. Kohonen, Self-Organization and Associative Memory, 3rd ed., Springer, Berlin, 1989.
[20] A. Sato, K. Yamada, Generalized Learning Vector Quantization, Advances in Neural Information Processing, vol. 8, MIT Press, Cambridge, MA, 1996, pp. 423–429.
[21] N.B. Karayiannis, J.C. Bezdek, N.R. Pal, R.J. Hahaway, P.I. Pai, Reapirs to glvq: A new family of competitive learning schemes, IEEE Transactions on Neural Networks 7 (5) (1996) 1062–1071.
[22] A.I. Gonzalez, M. Graña, A. D'Anjou, An analysis of the glvq algorithm, IEEE Transactions on Neural Networks 6 (4) (1995) 1012–1016.
[23] P.D. Wendt, E.J. Coyle, N.C. Gallagher, Stack filter, IEEE Transactions on Acoustics, Speech, Signal Processing ASSP-34 (4) (1986) 898–911.
[24] E.J. Coyle, J.H. Lin, Stack filters and the mean absolute error criterion, IEEE Transactions on Acoustics, Speech, Signal Processing ASSP-36 (1988) 1244–1254.
[25] C.C. Han, K.C. Fan, Finding of optimal stack filter by graphical searching methods, IEEE Transactions on Signal Processing 45 (7) (1997) 1857–1862.